



# Ground tire rubber composites with hybrid conductive network for efficiency electromagnetic shielding and low reflection

An Sheng<sup>1</sup> · Yaqi Yang<sup>1,2</sup> · Wei Ren<sup>1</sup> · Hongji Duan<sup>1,2</sup> · Baoying Liu<sup>3</sup> · Guizhe Zhao<sup>1</sup> · Yaqing Liu<sup>1</sup>

Received: 4 April 2019 / Accepted: 7 July 2019 / Published online: 11 July 2019  
© Springer Science+Business Media, LLC, part of Springer Nature 2019

## Abstract

An efficiency electromagnetic interference (EMI) shielding composite with low microwave reflection was fabricated by introducing nickel coated ultrahigh molecular weight polyethylene particles (UHMWPE@Ni) into ground tire rubber (GTR) matrix. Chain-like carbon black (CB) aggregates in GTR domains connected discontinuous Ni layers to form a hybrid conductive network. The remarkable EMI shielding effectiveness (SE) and low reflection characteristics of GTR/UHMWPE@Ni composites were attributed to the well-connected Ni–CB hybrid conductive network with both magnetic hysteresis loss and electrical loss, and the multi-interfaces structure induced by the selectively distributed Ni layer at the interface between UHMWPE and GTR. With only 1.04 vol% Ni content, the EMI SE of GTR/UHMWPE@Ni composite reached 47.3 dB in X band. Because of the synergistic effect of the Ni–CB hybrid network, the power coefficient of reflectivity (R) of the composite was as low as 0.58. The result indicated that our work provided a feasible strategy to fabricate efficient electromagnetic shielding materials with low microwave reflection.

## 1 Introduction

Over the past few decades, the serious electromagnetic radiation pollution has led to rapid development of conductive polymer composites (CPCs) for electromagnetic interference (EMI) shielding. Compared to traditional metal electromagnetic shielding materials, CPCs show significant development in the field of electromagnetic shielding due to their light weight, tunable conductivity, corrosion resistance and good processability [1–5]. In order to acquire CPCs with high EMI shielding effectiveness (SE), currently, novel conductive fillers with superior intrinsic electrical conductivity,

such as metal nanowires and MXenes, have been employed to provide the CPC shielding material with excellent conductivity [6, 7]. However, the excessive conductivity of these conductive fillers will cause high electromagnetic (EM) wave reflection due to the severe impedance mismatch, which would cause serious secondary EM radiation pollution and deteriorate electromagnetic environments. Carbon nanofillers, as the most widely used fillers for CPCs, are expected to attenuate EM waves mainly dominated by absorption rather than reflection [8, 9]. Regrettably, the single carbon nanofillers hardly afford magnetic hysteresis loss, which limits the microwave absorption ability for carbon-based CPCs. Therefore, the hybridization of magnetic metal and carbon fillers will be beneficial to obtain electromagnetic shielding material with both ideal EMI SE and low reflection [10].

Recently, modifying carbon fillers with magnetic particles has become an effective approach to reducing the wave reflection for CPC shielding materials. Reduced graphene oxide coated with magnetic Fe<sub>3</sub>O<sub>4</sub> or FeCo [11–13], multiwalled carbon nanotube plated with nickel or modified with Fe<sub>3</sub>O<sub>4</sub> are reported to reduce the EM wave reflection characterization of CPC shielding materials due to their magnetic and electrical loss [14, 15]. Among the magnetic fillers, Ni as a typical magnetic metal has already been combined with polymer bulk materials

✉ Hongji Duan  
duanhongji1983@163.com

✉ Yaqing Liu  
lyq@nuc.edu.cn

<sup>1</sup> College of Materials Science and Engineering, Key Laboratory of Functional Nanocomposites of Shanxi Province, North University of China, Taiyuan 030051, People's Republic of China

<sup>2</sup> State Key Laboratory of Polymer Materials Engineering, Sichuan University, Chengdu 610065, People's Republic of China

<sup>3</sup> Institute of Functional Polymer Composites, Henan University, Kaifeng 475004, People's Republic of China

or additives, or even in the form of nickel chains directly to afford effective EMI SE in polymer matrix [16–18]. Our previous work has constructed a 3D Ni conductive network in UHMWPE, and the 3D Ni structure with perfect conductive path could provide the composites with excellent electromagnetic shielding effectiveness at very low Ni content [19]. However, the single Ni conductive network still possesses high EM wave reflection due to its monotonous shielding mechanism. In view of the significant synergistic shielding effect between carbon and magnetic particles, the cooperation of Ni and carbon fillers is expected to reduce the reflection of Ni network and provide the CPCs with satisfied EMI shielding performance simultaneously [20, 21].

Ground tire rubber (GTR), a kind of granular material, is downsized from waste tire rubber and possesses intrinsic three-dimensional (3D) cross-linked structure that similar as high-viscosity gel. Besides, a mass of conductive carbon black (CB) spread over its interior and construct a conductive network [22–24]. Lately, Jia et al. reported a highly efficient GTR shielding composites with an EMI SE of 66.9 dB in X band, and confirmed that the CB located in the GTR domains plays an important role in constructing additional conductive networks and attenuating electromagnetic microwaves [25]. Therefore, the GTR can severe as a potential carbon conductive framework and offer an excellent opportunity to construct a “carbon-magnetic metal” hybrid shielding network by cooperating 3D Ni conductive network.

In this work, we adopt electroless deposition and compression molding method to fabricate GTR/UHMWPE@Ni composites with a hybrid network that consisted of Ni and CB. Due to the 3D cross-linked structure of GTR and high melting viscosity of UHMWPE, the Ni layers can selectively distribute between the boundaries of GTR and UHMWPE to form a hybrid conductive network with chain-like CB aggregates that located in GTR domains. The Ni layers play a role of attenuation centers to offer effective magnetic hysteresis loss and electrical loss, while the chain-like CB aggregates link these Ni attenuate centers to form a connected shielding network. Therefore, the GTR/UHMWPE@Ni composites with well-connected conductive network and magnetic loss exhibit high efficiency EMI SE and low reflection characteristics. With only 1.04 vol% Ni content, the EMI SE of GTR/UHMWPE@Ni composite reaches 47.3 dB in X band. Because of the synergistic effect of the Ni–CB hybrid network, the power coefficient of reflectivity ( $R$ ) of the composite is as low as 0.58. This exciting result indicates that our work provides a feasible strategy to significantly reduce microwave reflection when fabricating efficient EMI shielding materials. It is worth mentioning that the introduction of GTR not only contributes to the excellent performance of the GTR/UHMWPE@Ni composites, but also conduces to relieve heavy burden from the pollution of waste tire rubber.

## 2 Experiment

### 2.1 Materials and preparation

GTR with 60 mesh size and composed of 62.8 wt% hydrocarbon, 13.4 wt% carbon black, 23.8 wt% ash, was provided by the Sichuan Zhongneng Rubber Co. LTD., China, UHMWPE granules with average diameter of 150  $\mu\text{m}$ , density of 0.94  $\text{g}/\text{cm}^3$ , and melting temperature of 137  $^\circ\text{C}$  were supplied by Beijing No.2 Auxiliary Agent Factory. The reagents used in electroless deposition process included  $\text{H}_2\text{SO}_4$  (98 wt%),  $\text{SnCl}_2 \cdot 2\text{H}_2\text{O}$  ( $\geq 98.0\%$ ),  $\text{HCl}$  (38.0%),  $\text{PdCl}_2$  ( $\geq 99.9\%$ ),  $\text{NH}_3 \cdot \text{H}_2\text{O}$  (28%),  $\text{NiCl}_2 \cdot 6\text{H}_2\text{O}$  ( $\geq 98.0\%$ ),  $\text{NaH}_2\text{PO}_2 \cdot \text{H}_2\text{O}$  ( $\geq 99.0\%$ ),  $\text{C}_6\text{H}_5\text{Na}_3\text{O}_4 \cdot 2\text{H}_2\text{O}$  ( $\geq 99.0\%$ ). All chemical reagents, purchased from Kaitong Chemical Reagent Co. LTD (Tianjin, China), were of analytical grade and used without further purification.

The fabrication process of the GTR/UHMWPE@Ni composites is illustrated in Fig. 1. UHMWPE@Ni particles with the Ni content of 18.2 wt% were prepared by electroless deposition according to the method reported in our previously work [26]. Then, the UHMWPE@Ni particles were mixed with GTR at different weight ratio. Afterwards, the mixture was hot pressed into sheet with a thickness of 2 mm under the pressure of 30 MPa at 175  $^\circ\text{C}$  for 20 min, and then cooled to room temperature to proceed cold compression molding for 5 min. This method can induce interchange reactions of polysulfide crosslinks to generate new sulfidic crosslinks at high temperature [27], thereby the GTR particles are sintered into matrix materials. In addition, the bonding between different matrix regions can be enhanced at high pressure due to the increased interparticle contact area and consequent allowance of segmental diffusion of rubber molecules at the particle interfaces [27, 28].

### 2.2 Characterization

The Ni layer structure of UHMWPE@Ni particles was determined by X-ray diffraction (XRD, Haoyuan 2700B) using  $\text{Cu K}\alpha$  ( $k = 0.1546 \text{ nm}$ ). Magnetic properties were measured at room temperature using vibrating sample magnetometer (VSM, Microsense FCM-10). A field emission scanning electron microscopy (FESEM, Hitachi SU8010) was used for morphology observations at the accelerated voltage of 10 kV. Before SEM observation, the GTR/UHMWPE@Ni composites were clipped into slices with 15  $\mu\text{m}$  thickness by an ultramicrotome (Leica EM UC-7) and sputter-coated with gold. The distribution of fillers in the composites was investigated via energy dispersive spectrometer (EDS). A four-point probes meter

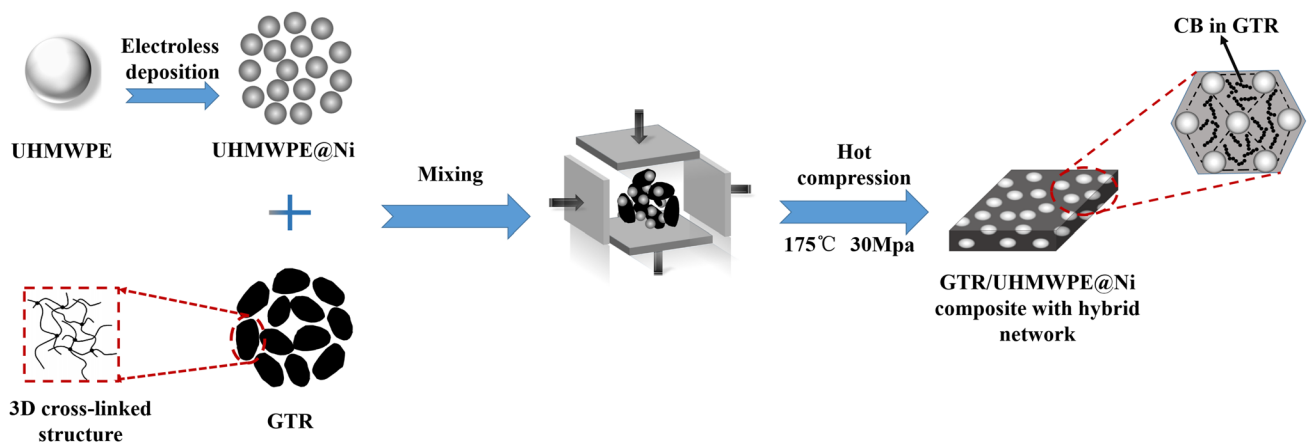


**Fig. 1** Schematic for the fabrication of GTR/UHMWPE@Ni composite

(Probers tech RTS-9) was employed to detect electrical conductivity if the electrical conductivity of composites higher than  $10^{-6}$  S/m, while the conductivity lower than  $10^{-6}$  S/m were detected via a high-resistance meter (Shanghai Precision ZC36). EMI SE of the composites were measured by using a vector network analyzer (VNA, Agilent N5232A) with a coaxial test cell (APC-7connector) in conjunction according to ASTM ES7-83. All the samples with 15 mm diameter and 2 mm thickness were placed in the specimen holder. The measured scattering parameters ( $S_{11}$  and  $S_{21}$ ) were used to calculate the EMI SE. From the measured scattering parameters ( $S_{11}$  and  $S_{21}$ ), the total EMI SE ( $SE_{\text{Total}}$ ), shielding effectiveness of the absorption ( $SE_A$ ), reflection ( $SE_R$ ), multiple internal reflections ( $SE_M$ ) and power coefficients of reflectivity ( $R$ ), transmissivity ( $T$ ), and absorptivity ( $A$ ) could be obtained as follow [29]:

$$R = |S_{11}|^2 \quad (1)$$

$$T = |S_{21}|^2 \quad (2)$$

$$A = 1 - R - T \quad (3)$$

$$SE_R = -10\lg(1 - R) \quad (4)$$

$$SE_A = -10\lg(T/(1-R)) \quad (5)$$

$$SE_{\text{Total}} = SE_R + SE_A + SE_M \quad (6)$$

### 3 Results and discussion

#### 3.1 Characterization of UHMWPE@Ni particles and GTR

The SEM observation of UHMWPE@Ni particles are shown in Fig. 2a. A nickel layer has been uniformly deposited on the surface of UHMWPE after electroless plating. The high magnification images (Fig. 2b, c) exhibit that the Ni layer of the UHMWPE@Ni particles are rather dense and compact. Figure 2d, e displays the surface morphology of GTR particles, and the irregular shapes with rough surfaces are beneficial for GTR to obtain larger specific surface area. From the SEM image of pristine GTR in high magnification (Fig. 2f), many agminated CB particles are visually shown in the interior of the GTR matrix. These CB agglomerates with chain-like structure can serve as a potential carbon conductive framework, and are expected to impart outstanding electrical and EMI shielding performance for the GTR/UHMWPE@Ni composites by further cooperating with Ni conductive network. The XRD pattern of UHMWPE@Ni particles are exhibited in Fig. 2g. The three typical characteristic peaks at  $2\theta = 44.5^\circ$ ,  $51.8^\circ$  and  $76.4^\circ$  are consistent with the diffraction of (111), (200), and (220) crystallized planes of Ni, which in accordance with the standard metallic face-centered cubic (fcc) structure (JCPDS no. 04-0850). It means that a nickel layer has successfully formed on the surface of UHMWPE. In electroless deposition process, the sodium hypophosphite ( $\text{NaH}_2\text{PO}_2$ ) is used as reducing agent to reduce nickel salts, so the reaction product contains a small amount of phosphorus-containing compound. According to JCPDS 74-1381, the diffraction peak at  $38.4^\circ$  belongs to the (112) crystallized planes of the tetragonal phase of  $\text{Ni}_{12}\text{P}_5$  [30]. Magnetic hysteresis loops of UHMWPE@Ni particles and GTR/UHMWPE@Ni composites are shown in Fig. 2h. The saturation magnetization

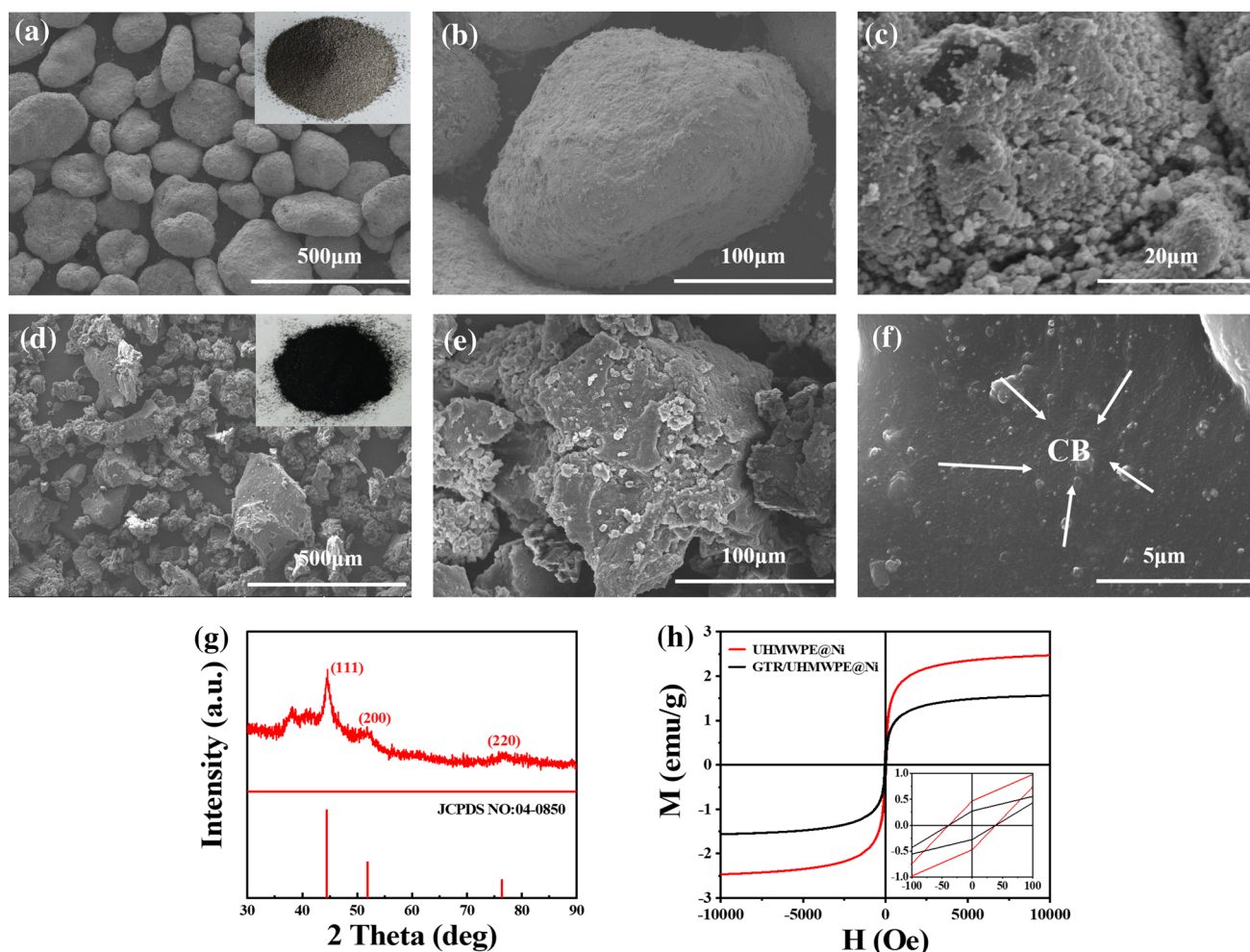


**Fig. 2** **a** SEM images of UHMWPE@Ni particles, the inset is optical image of UHMWPE@Ni, **b**, **c** high magnification images of **(a)**, **d** SEM images of GTR particles, the inset is optical image of GTR, **e** high magnification image of **(d)**, **f** CB in GTR domains, **g** XRD

pattern of UHMWPE@Ni particles. **h** Magnetic hysteresis loops of UHMWPE@Ni particles and GTR/UHMWPE@Ni composites with 0.71 vol% Ni content

of GTR/UHMWPE@Ni composites is lower than that of UHMWPE@Ni due to the introduction of nonmagnetic GTR matrix. With 0.71 vol% Ni content, the saturation magnetization and coercivity are 1.57 emu/g and 40 Oe, respectively.

### 3.2 Microstructure of GTR/UHMWPE@Ni composites

Figure 3a–d show the fractured surface microstructures of GTR/UHMWPE@Ni composites with various Ni content. The UHMWPE@Ni is surrounded with GTR domains and dispersed uniformly in the composites. As shown in Fig. 3a–c, the Ni layers are isolated distribution between UHMWPE and GTR region, failing to build a continuous conductive network due to the large distance between UHMWPE@Ni particles. With the increased content of UHMWPE@Ni particles, more physical connections of Ni layers can be observed, which means that the Ni conductive network is

gradually completed in the GTR/UHMWPE@Ni composites. When the volume fraction of Ni increase to 1.04 vol% (Fig. 3d), the dense UHMWPE@Ni particles are close enough to construct a continuous Ni conductive network in the matrix.

Figure 3e, f reveal that the Ni layers are located at the interface between GTR (black circles) and UHMWPE (yellow circles) domains. The EDS mapping of Ni element (Fig. 3h) manifests that the Ni fillers distribute on the surface of UHMWPE particles. The coherent Ni layers have formed conductive paths along the interfaces of UHMWPE and GTR, without penetrating into UHMWPE regions or GTR regions. This is mainly due to the specific high viscosity of melting UHMWPE during compression molding process, which allow the prearranged nickel layer only selectively locate at the boundary. Meanwhile, the GTR with original 3D cross-linked structure prevents the Ni layers

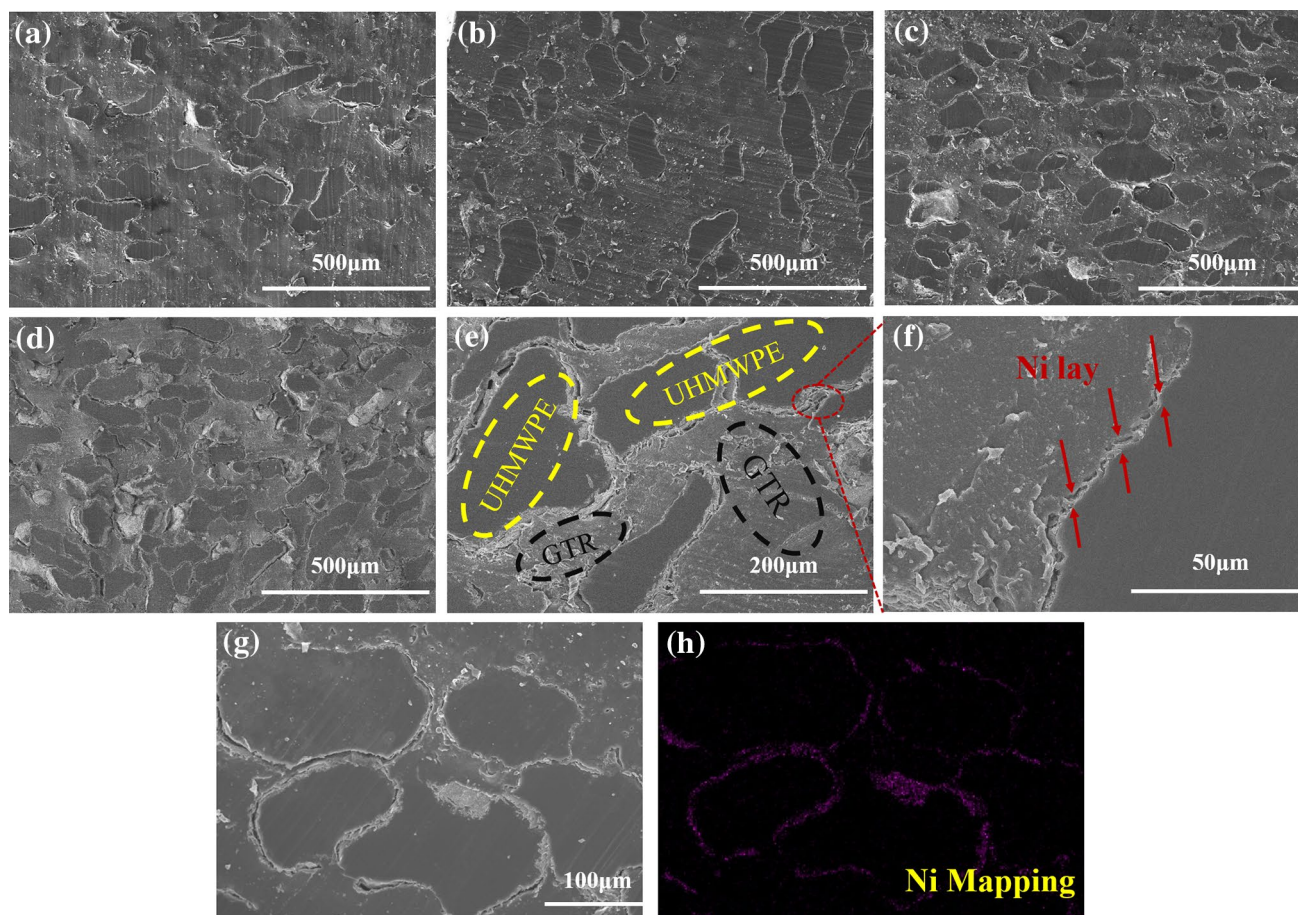


**Fig. 3** SEM micrographs of GTR/UHMWPE@Ni composites with various Ni loading: **a** 0.44 vol%, **b** 0.54 vol%, **c** 0.71 vol% and **d** 1.04 vol%; **e** and **f** are the magnified images of **(d)**, **g** fracture surface of

GTR/UHMWPE@Ni composites and **h** corresponding Ni elemental mapping (Color figure online)

from penetrating into GTR regions by extremely confining the movement of macromolecular chains [31, 32]. Hence the agminated CB with chain-like structure in the interior of GTR could connect UHMWPE@Ni regions to form a novel hybrid network that consist of carbon and Ni. Due to the inherent existence of CB in the matrix, a complete conductive network can be formed more easily at very low Ni content. Thus, the GTR/UHMWPE@Ni composites are expected to exhibit preeminent conductivity and high-efficiency EMI SE with the synergistic effect of CB and Ni hybrid conductive network.

### 3.3 Electrical conductivity of GTR/UHMWPE@Ni composites

The electrical conductivity of the GTR/UHMWPE@Ni composites with different Ni content (vol%) are demonstrated in Fig. 4. The conductivity of the composites significantly increases with the improved Ni content. Due to the presence of chain-like CB agglomerates, the electrical conductivity

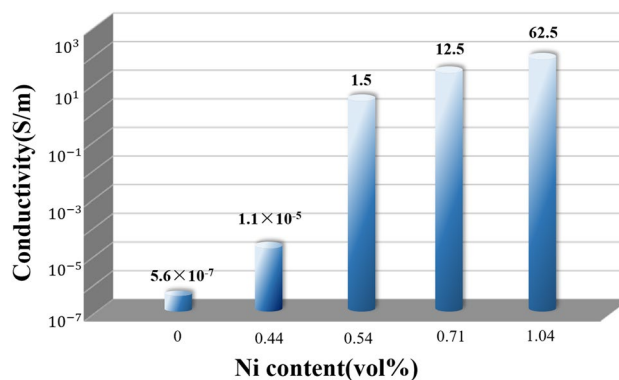


**Fig. 4** Electrical conductivities of pristine GTR and GTR/UHMWPE@Ni composites with various Ni loading

of pristine GTR is  $5.6 \times 10^{-7}$  S/m. By loading only 0.54 vol% Ni, the conductivity can be significantly increased to 1.2 S/m. When the content of Ni further increases to 1.04 vol%, the electrical conductivity reaches 62.5 S/m, which is

8 orders of magnitude higher than that of the pristine GTR. Such a significant increase should be ascribed to the selective distribution of Ni layers and the hybrid conductive network with the participation of CB. Owing to the high viscosity of UHMWPE and inherent 3D cross-linked structure of GTR matrix, there exists a conspicuous “excluded volume” effect in the composites, hence the Ni layers are regularly distributed at the interfaces [33]. On the other hand, numerous CB in GTR matrix can provide additional conductive path between UHMWPE@Ni particles to build more completed and efficient conductive network [25]. Therefore, the composites possess ideal electrical conductivity even at very low Ni content. Undoubtedly, this specific hybrid network structure is beneficial for GTR/UHMWPE@Ni composites to attain high-efficiency EMI shielding performance.

### 3.4 EMI SE of GTR/UHMWPE@Ni composites

The EMI SE of GTR/UHMWPE@Ni composites as a function of Ni content in the frequency range of 8.2–12.4 GHz (X-band) is shown in Fig. 5a. Apparently, the EMI SE is strongly associated with the Ni content, and scarcely exhibits frequency dependence over the whole frequency range. The EMI SE of pristine GTR is relatively low due to the low conductivity of single CB network. However, after the addition of Ni, the EMI SE of the GTR/UHMWPE@Ni composites increases significantly with the improved Ni content due to the gradually completed Ni–CB hybrid conductive network. At the Ni content of 0.54 vol%, the composite exhibits an EMI SE of 25.3 dB, which already exceeds the commercial application requirement of 20 dB. When Ni loading reaches 1.04 vol%, the average EMI SE of the composite can achieve 47.3 dB, which means 99.998% of the incident electromagnetic waves can be blocked. This remarkable enhancement is mainly attributed to the synergism between CB and Ni in hybrid conductive network. Due to the presence of CB, GTR is actually served as a percolated polymer matrix, and can greatly promote the establishment of perfect conductive network with the participation of Ni. This perfect hybrid

conductive network is highly beneficial to high electrical conductivity and thus leads to highly efficient EMI shielding performance. Moreover, the Ni layers with both magnetic and electrical properties served as EM wave attenuation centers also enhance the EMI shielding capacity effectively.

In order to distinctly illuminate the EMI shielding mechanism of this Ni–CB hybrid network, the  $SE_A$  and  $SE_R$  of the composites are analyzed and shown in Fig. 5b. It is obviously that the  $SE_A$  rises sharply with the increase of Ni content. Generally, the  $SE_R$  always increases along with the electrical conductivity due to the enhancement of wave reflection that caused by the increased impedance mismatching [34]. However, the  $SE_R$  of the GTR/UHMWPE@Ni composites is not improved but even downward with the increased Ni content at a certain range. According to Fig. 5b, when the loading of Ni is 0.54 vol%, the  $SE_A$  and  $SE_R$  are 21.2 dB and 4.1 dB, which means that the contribution of  $SE_A$  to the entire shielding effectiveness is 83.8%. As the Ni content increases to 0.71 vol%, the contribution of  $SE_A$  (27.0 dB) to the entire shielding effectiveness is enhanced to 87.7%, while the  $SE_R$  drops to only 3.8 dB. This phenomenon indicates that the addition of Ni completely increases the absorption rather than reflection. The improvement of  $SE_{Total}$  of the composites is mainly attributed to the enhancement of waves absorption that induced by the synergistic effect of Ni and CB. Consequently, with the specific design of carbon–metal hybrid network, the absorption attenuation capacity of GTR/UHMWPE @Ni composites can be significantly improved in X band.

To further comprehend the influence of the hybrid network to EMI shielding performance, the relationship between power coefficients [i.e. reflectivity (R) and absorptivity(A)] and Ni content are illustrated in Fig. 6a. The pristine GTR shows a high average R value of 0.76. When Ni loading is 0.44 vol%, the R value drops to 0.60. As the Ni content increases to 0.71 vol%, the R values is 0.58. This is a very interesting phenomenon and the result is superior to most EMI shielding materials at similar EMI SE value [8, 17, 35–40]. The evident downtrend of R convincingly

**Fig. 5** a EMI SE of GTR/UHMWPE@Ni composites as a function of frequency in X-band range; b  $SE_R$ ,  $SE_A$ , and  $SE_{Total}$  of GTR/UHMWPE@Ni composites with various Ni content

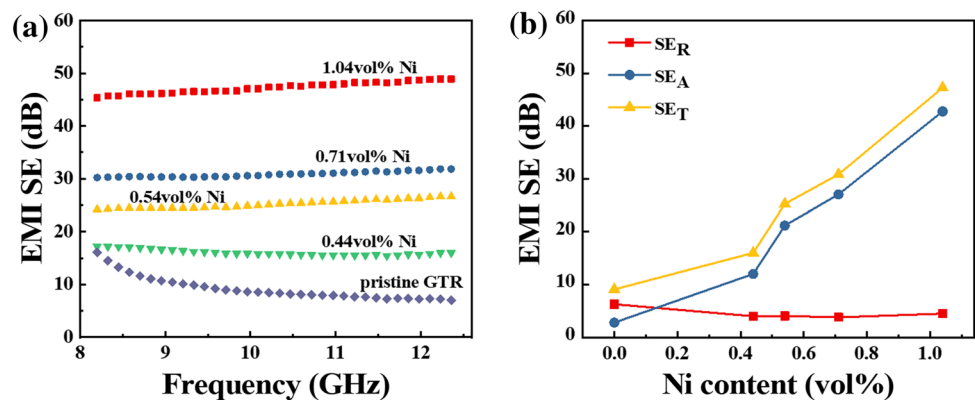
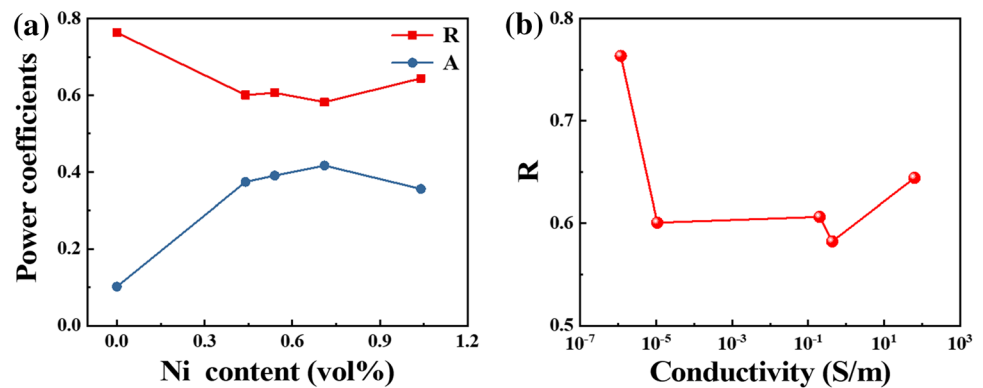


**Fig. 6** **a** Power coefficient of reflectivity (R) and absorptivity (A) of GTR/UHMWPE@Ni composites with various Ni loading; **b** R value as a function of conductivity



indicates that the hybrid network is able to decrease the reflection effectively. The reasons of such low reflection of GTR/UHMWPE@Ni composites can be ascribed to three factors: first, the magnetic Ni could absorb EM waves through magnetic hysteresis loss and electrical loss in the hybrid conductive network. Since the conductivity of the composite is relatively low before the Ni fillers connect with each other to form a conductive network, EM waves have more opportunity to enter into the interior of the composites and then be attenuated via magnetic hysteresis loss and electrical loss. Hence the wave absorption is improved and wave reflection is reduced with the raised Ni loading before the formation of continuous Ni conductive network. In this case, wave absorption would provide notable effect to induce low reflection. As proved in Fig. 6b, R decreases initially and then increases with the improvement of conductivity, the raised conductivity means that the Ni layers transform from discontinuous to continuous. The raised conductivity means that the Ni layers transform from discontinuous to continuous. Once the Ni fillers connect with each other to form a continuous and complete conductive network, the significantly improved conductivity causes great reflection. Consequently, a large proportion of electromagnetic waves is reflected back at the surface of composites, and the reflection could significantly surpass the absorption to become the dominant shielding mechanism. Therefore, the R value shows a minimum value with 0.71 vol% of Ni, and then increased when Ni content is 1.04 vol%. Secondly, the hybrid network creates a multi-interfaces structure by embedding UHMWPE@Ni particles into GTR domains. As a result, there are plentiful interfaces among Ni, UHMWPE and GTR. The interfacial polarization originated from these interfaces can greatly promote the absorption when the EM waves penetrate into the composites [41]. Finally, the CB particles in GTR domains can act as conductive centers that interact with the EM waves, leading to a further enhancement of wave absorption [25].

The complex permittivity and complex permeability of pristine GTR, GTR/UHMWPE@Ni composites and UHMWPE@Ni composites are investigated in Fig. 7. According

to Debye theory, the complex permittivity ( $\epsilon = \epsilon' - j\epsilon''$ ) and complex permeability ( $\mu = \mu' - j\mu''$ ) determine the microwave absorption ability, the real part ( $\epsilon'$  and  $\mu'$ ) symbolize the storage ability of electric and magnetic energy while the imaginary part ( $\epsilon''$  and  $\mu''$ ) symbolize the dissipation. The dielectric loss tangent ( $\tan\delta = \epsilon''/\epsilon'$ ) and magnetic loss tangent ( $\tan\delta = \mu''/\mu'$ ) are also calculated according to the values of complex permittivity and permeability. As exhibited in Fig. 7c and f, the pristine GTR material with low electrical conductivity and negligible magnetism exhibits inferior dielectric loss and magnetic loss. After the electromagnetic dual functional UHMWPE@Ni particles are added into GTR matrix and distributed independently (0.71 vol% Ni content), the dielectric loss and magnetic loss are significantly enhanced. For UHMWPE@Ni composite with higher conductivity (Fig. 8), the dielectric loss and magnetic loss are lower than those of GTR/UHMWPE@Ni composite. The interesting phenomenon confirms that the excessive electrical conductivity of perfect Ni conductive network reduces the dielectric loss and magnetic loss and thus increases the R value of the composites. Moreover, the highest electromagnetic parameters and lowest R value of GTR/UHMWPE@Ni composite demonstrate that the Ni–CB hybrid network can exhibit significant synergy to low reflection characteristic.

The EMI shielding mechanism of the GTR/UHMWPE@Ni composites is schematically presented in Fig. 9. Numerous chain-like CB aggregates in GTR domains connect discontinuous Ni layers to form a hybrid conductive network. Since the highly conductive Ni is wrapped by the GTR matrix with a lower conductivity, more electromagnetic waves can penetrate into the composite due to the mitigation of impedance mismatching. The “UHMWPE–Ni–GTR” multi-interfaces structure in the composite repeatedly interacts with incident EM waves via interfacial polarization and multiply reflection to attenuate microwaves. Moreover, the presence of Ni layers also provides considerable magnetic hysteresis loss, which further increases the absorption attenuation. As a result, the GTR/UHMWPE@Ni composites can exhibit high-efficiency EMI SE and low-reflection characteristic due to this magnetic metal–carbon hybrid network.

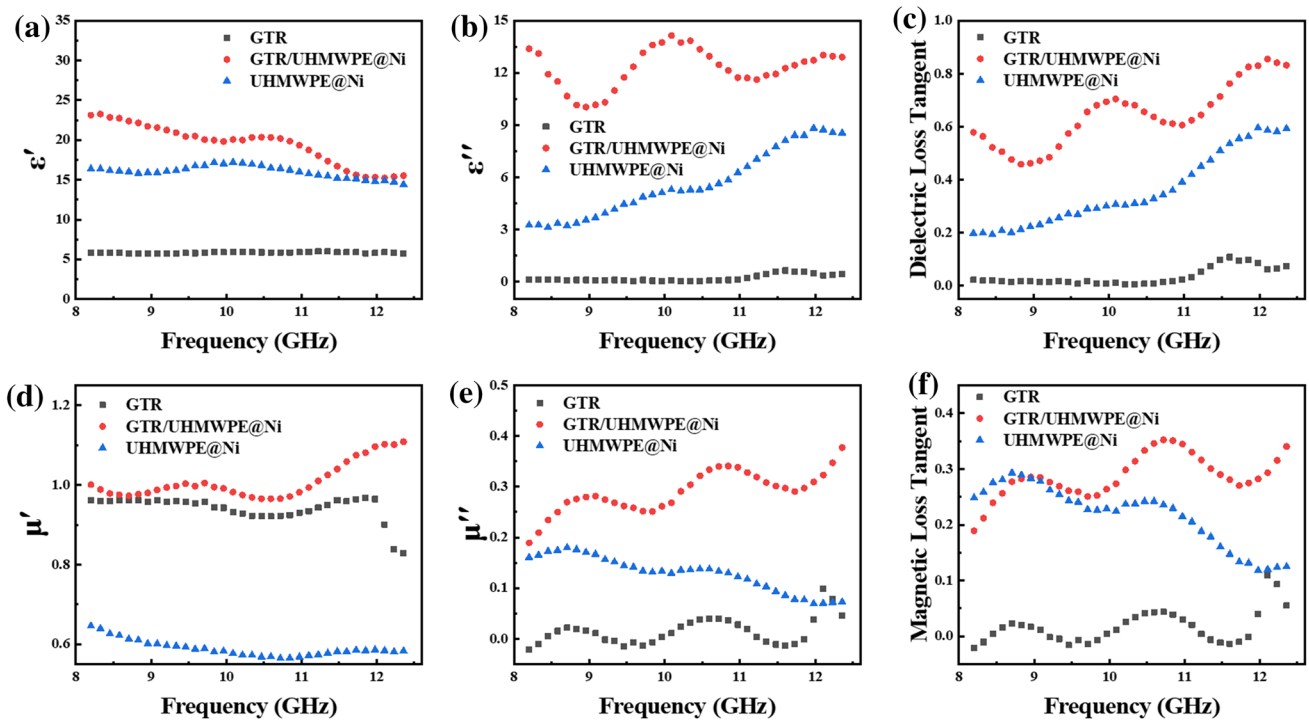


**Fig. 7** **a** Real and **b** imaginary parts of the complex permittivity, **c** dielectric loss tangent, **d** real parts and **e** imaginary parts of the complex permeability, and **f** magnetic loss tangent for pristine GTR, GTR/UHMWPE@Ni composite and UHMWPE@Ni composite

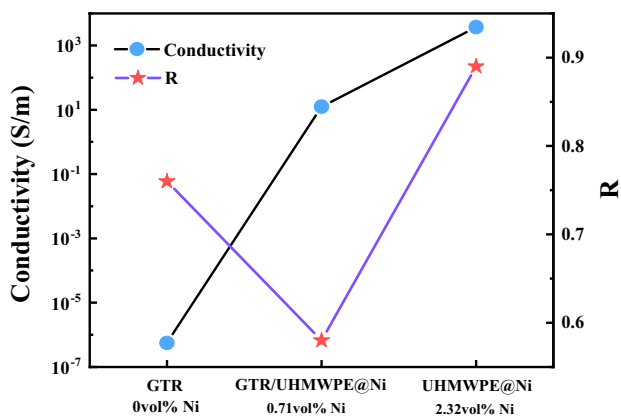


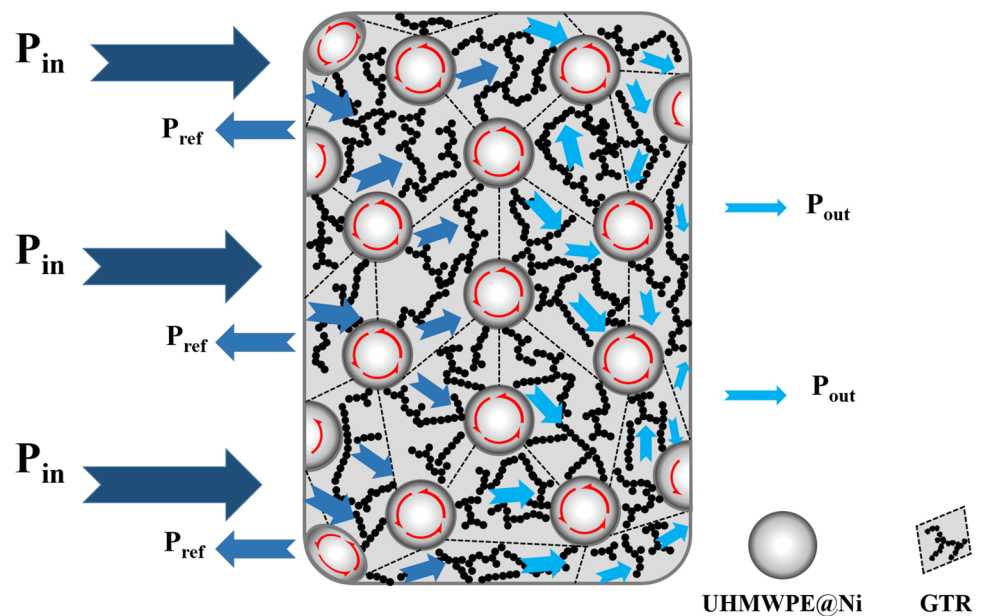
**Fig. 8** The electrical conductivity and power coefficient of reflectivity (R) of pristine GTR, GTR/UHMWPE@Ni composite and UHMWPE@Ni composite

## 4 Conclusions

The GTR/UHMWPE@Ni composites with high-efficiency EMI SE and low-reflection characteristic have been prepared in this work. Chain-like CB aggregates in GTR domains connect discontinuous Ni layers to form a hybrid conductive network. With only 1.04 vol% Ni content, the EMI SE of GTR/UHMWPE@Ni composite reaches 47.3 dB in X band. Because of the synergistic effect of the Ni–CB hybrid network, the R value of the composite is as low as 0.58. This performance demonstrates that our work provides a simple and feasible strategy to fabricate the novel shielding composites which not only do well at the attenuation of electromagnetic wave but also prominently alleviate serious secondary EM reflection pollution.



**Fig. 9** Schematic representation of the EMI shielding mechanism for the GTR/UHMWPE@Ni composites with hybrid network



**Acknowledgements** The authors gratefully acknowledge the financial support from the National Natural Science Foundation of China (Grant No. 21704070), Natural Science Foundation of Shanxi Province (Grant Nos. 201701D221089; 201801D121109), and the Opening Project of State Key Laboratory of Polymer Materials Engineering (Sichuan University) (Grant Nos. sklpm2017409; sklpm2018-4-35). We are also grateful for the support from Shanxi Province 1331 Project Key Innovation Team of Polymeric Functional New Materials, Shanxi Province Innovative Disciplinary Group of New Materials Industry, and Shanxi Province Patent Conversion Project (Grant No. 20171007).

## References

- B. Shen, W.T. Zhai, M.M. Tao, J.Q. Ling, W.G. Zheng, *ACS Appl. Mater. Interfaces* **5**, 11383–11391 (2013)
- N. Yousefi, X. Sun, X. Lin, X. Shen, J. Jia, B. Zhang, B. Tang, M. Chan, J.K. Kim, *Adv. Mater.* **26**, 5480–5487 (2014)
- D.X. Yan, H. Pang, B. Li, R. Vajtai, L. Xu, P.G. Ren, J.H. Wang, Z.M. Li, *Adv. Funct. Mater.* **25**, 559–566 (2015)
- Y. Wang, J. Hao, Z. Huang, G. Zheng, K. Dai, C. Liu, C. Shen, *Carbon* **126**, 360–371 (2018)
- X. Wei, X. Cao, Y. Wang, G. Zheng, K. Dai, C. Liu, C. Shen, *Compos. Sci. Technol.* **149**, 166–177 (2017)
- Y. Wang, F.Q. Gu, L.J. Ni, K. Liang, K. Marcus, S.L. Liu, F. Yang, J.J. Chen, Z.S. Feng, *Nanoscale* **9**, 18318–18325 (2017)
- J. Liu, H.B. Zhang, R. Sun, Y. Liu, Z. Liu, A. Zhou, Z.Z. Yu, *Adv. Mater.* **29**, 1702367 (2017)
- Z. Zeng, M. Chen, H. Jin, W. Li, X. Xue, L. Zhou, Y. Pei, H. Zhang, Z. Zhang, *Carbon* **96**, 768–777 (2016)
- S. Zhao, L. Yan, X. Tian, Y. Liu, C. Chen, Y. Li, J. Zhang, Y. Song, Y. Qin, *Nano. Res.* **11**, 530–541 (2017)
- W. Xu, Y.F. Pan, W. Wei, G.S. Wang, *A.C.S. Appl. Nano Mater.* **1**, 1116–1123 (2018)
- Y. Xu, Y. Yang, D.X. Yan, H. Duan, G. Zhao, Y. Liu, *A.C.S. Appl. Mater. Interfaces* **10**, 19143–19152 (2018)
- H. Zhu, Y. Yang, A. Sheng, H. Duan, G. Zhao, Y. Liu, *Appl. Surf. Sci.* **469**, 1–9 (2019)
- Y. Zheng, Y. Li, Z. Li, Y. Wang, K. Dai, G. Zheng, C. Liu, C. Shen, *Compos. Sci. Technol.* **139**, 64–73 (2017)
- J. Li, Y. Xie, W. Lu, T.W. Chou, *Carbon* **129**, 76–84 (2018)
- Y.J. Yim, K.Y. Rhee, S.J. Park, *Compos. Part B* **98**, 120–125 (2016)
- Y. Xu, Y. Yang, H. Duan, J. Gao, D.X. Yan, G. Zhao, Y. Liu, *Appl. Surf. Sci.* **455**, 856–863 (2018)
- B. Zhao, S. Wang, C. Zhao, R. Li, S.M. Hamidinejad, Y. Kazemi, C.B. Park, *Carbon* **127**, 469–478 (2018)
- Y. Xu, Y. Yang, D. Yan, H. Duan, C. Dong, G. Zhao, Y. Liu, *J. Mater. Sci.* **28**, 9126–9131 (2017)
- H. Duan, Y. Xu, D.X. Yan, Y. Yang, G. Zhao, Y. Liu, *Mater. Lett.* **209**, 353–356 (2017)
- H.X. Zhu, Y.Q. Yang, H.J. Duan, G. Zhao, Y. Liu, *J. Mater. Sci.* **30**, 2045–2056 (2018)
- H.J. Duan, H.X. Zhu, J.M. Yang, J.F. Gao, Y. Yang, G. Zhao, Y. Liu, *Compos. Part A* **118**, 41–48 (2018)
- K. Aoudia, S. Azem, N. Hocine, M. Gratton, V. Pettarin, S. Seghar, *Waste Manag.* **60**, 471–481 (2017)
- B. Sripornsawat, S. Saiwari, S. Pichaiyut, C. Nakason, *Eur. Polym. J.* **85**, 279–297 (2016)
- S. Ramarad, M. Khalid, C.T. Ratnam, A.L. Chuah, W. Rashmi, *Prog. Mater. Sci.* **72**, 100–140 (2015)
- L.C. Jia, Y.K. Li, D.X. Yan, *Carbon* **121**, 267–273 (2017)
- J. Yang, Y. Yang, H. Duan, G. Zhao, Y. Liu, *J. Mater. Sci.* **28**, 5925–5930 (2016)
- E. Bilgili, A. Dybek, H. Arastoopour, B. Bernstein, *J. Elastom. Plast.* **35**, 235–256 (2003)
- S. Tamura, K. Murakami, H. Kuwazoe, *J. Appl. Polym. Sci.* **28**, 3467–3484 (1983)
- L.C. Jia, D.X. Yan, X. Liu, R.J. Ma, H. Wu, Z.M. Li, *A.C.S. Appl. Mater. Interfaces* **14**, 11941–11949 (2018)
- H.Z. Wan, L. Li, Y. Chen, J.L. Gong, M.Q. Duan, C. Liu, J. Zang, H. Wang, *Electrochim. Acta* **229**, 380–386 (2017)
- H. Pang, L. Xu, D.X. Yan, Z.M. Li, *Conductive polymer composites with segregated structures. Prog. Polym. Sci.* **39**, 1908–1933 (2014)
- L.C. Jia, D.X. Yan, C.H. Cui, X. Jiang, X. Ji, Z.M. Li, *J. Mater. Chem. C* **3**, 9369–9378 (2015)

33. K. Zhang, G.H. Li, L.M. Feng, N. Wang, J. Guo, K. Sun, K.X. Yu, J.B. Zeng, T. Li, Z. Guo, M. Wang, *J. Mater. Chem. C* **5**, 9359–9369 (2017)
34. M.H. Al-Saleh, U. Sundararaj, *Carbon* **47**, 1738–1746 (2009)
35. K. Zhang, H.O. Yu, K.X. Yu, Y. Gao, M. Wang, J. Li, S. Guo, *Compos. Sci. Technol.* **156**, 136–143 (2018)
36. J.F. Gao, J.C. Luo, L. Wang, X.W. Huang, H. Wang, X. Song, M.J. Hu, L.C. Tang, H.G. Xue, *Chem. Eng. J.* **364**, 493–502 (2019)
37. Z. Zeng, H. Jin, M. Chen, W. Li, L. Zhou, Z. Zhang, *Adv. Funct. Mater.* **26**, 303–310 (2016)
38. H.Y. Wu, L.C. Jia, D.X. Yan, J.F. Gao, X.P. Zhang, P.G. Ren, Z.M. Li, *Compos. Sci. Technol.* **156**, 87–94 (2018)
39. Z. Zeng, C. Wang, Y. Zhang, P. Wang, S.I. Shahabadi, Y. Pei, M. Chen, X. Lu, *A.C.S. Appl. Mater. Interfaces* **10**, 8205–8213 (2018)
40. F. Ren, D. Song, Z. Li, L. Jia, Y. Zhao, D. Yan, P. Ren, *J. Mater. Chem. C* **6**, 1476–1486 (2018)
41. B. Zhao, X. Guo, W. Zhao, J. Deng, G. Shao, B. Fan, Z. Bai, R. Zhang, *A.C.S. Appl. Mater. Interfaces* **8**, 28917–28925 (2016)

**Publisher's Note** Springer Nature remains neutral with regard to jurisdictional claims in published maps and institutional affiliations.